Supporting Information

Sub-nano molybdenum oxide nanoring as amplified atomic-efficiency sonosensitizers for highly efficient sonodynamic tumor ablation

Wanying Zhang [a], Kaidi Liang [a], Pengyu Zang [a], Rui Zhang [a], Chenghao Yu [a], Lei Zhong [b], Yushan Dong*[,a], Dan Yang*[,a], and Piaoping Yang*[,a]

[a] Key Laboratory of Superlight Materials and Surface Technology, Ministry of Education, College of Material Sciences and Chemical Engineering, Harbin Engineering University, Harbin, 150001, P. R. China

E-mail: dongyushan@hrbeu.edu.cn; yangdan@hrbeu.edu.cn; yangpiaoping@hrbeu.edu.cn

[b] Department of Breast Surgery, Sixth Affiliated Hospital of Harbin Medical University, Harbin, 150023, P. R. China

EXPERIMENTAL SECTION

Materials and Reagents. Ammonium heptamolybdate [$(NH_4)_6Mo_7O_{24}\cdot 4H_2O$], thiourea, Oleylamine (OM), oleyl alcohol (OA) and polyethyleneimine (PEI) were purchased from Sinopharm Chemical Reagent Beijing Co., Ltd. 1,3-diphenylisobenzofuran (DPBF), 3,3′,5,5′-tetramethyl-benzidine (TMB), nitrotetrazolium blue chloride (NBT), 2,2,6,6-tetramethylpiperidine (TEMP), 5,5-dimethyl-1pyrroline N-oxide (DMPO) were purchased from Sigma-Aldrich. 2′,7′-dichlorofluorescein diacetate (DCFH-DA), methylthiazolyldiphenyl-tetrazolium bromide (MTT), DAPI, Calcein-AM and propidium iodide (PI) were obtained from Aladdin (Shanghai, China). PBS and trypsin cell digestive juices were purchased from Gibco Life Technologies. The JC-1 staining kit was obtained from Beyotime Inst. Biotech., (Haimen, China). Annexin V-FITC/PI apoptosis detection kit was taken from Tianjin Sungene Biotech Co., Ltd. (Tianjin, China). The TUNEL (TdT-mediated dUTP nick-end labeling) cell apoptosis detection kit was bought from Dalian Meilun Biotechnology Co., Ltd.

Experimental Apparatus. The transmission electron microscopy (TEM) image was obtained from the FEI Tecnai T20 transmission electron microscope. X-ray diffraction (XRD) was measured by a Rigaku DMAX-2400 X-ray diffractometer equipped with Cu Kα radiation (λ = 0.154 nm) at 40 kV and 40 mA. X-ray photoelectron spectroscopy (XPS) was measured by Thermo Fisher Scientific ESCALAB 250XI. Inductively coupled plasma mass spectrometry (ICP-MS) was performed by Agilent Technologies 725. UV-vis absorption spectrum was carried out by UV-1601 spectrophotometer. The

zeta potential measurement of different samples was performed on a Malvern Zetasizer Nan Nano ZS90. UV-vis diffuse reflectance spectrum was tested by Shimadzu UV3600. The ESR spectra were obtained with a Bruker EMX1598 spectrometer. The flow cytometry assays were conducted on a BD Accuri C6 flow cytometer (USA). A confocal laser scanning microscopy (CLSM, Leica TCS SP8) was used to obtain the fluorescence image.

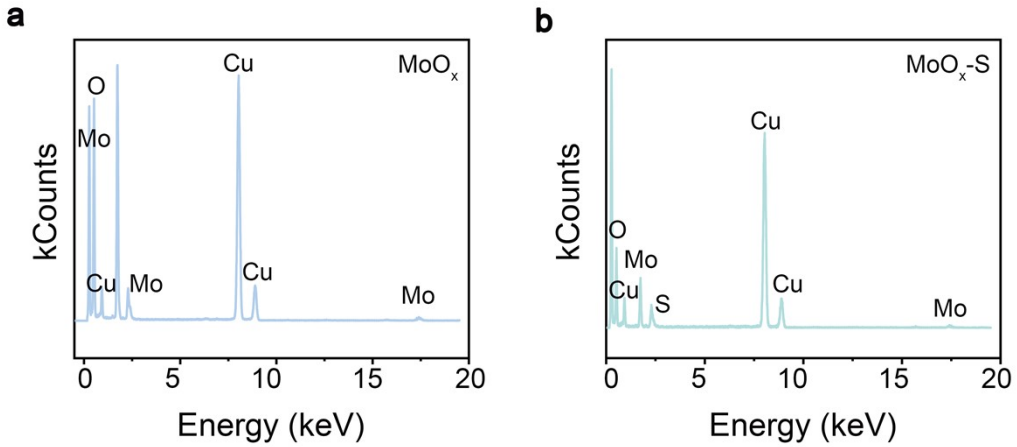

Figure S1. EDS of MoO_x NPs and MoO_x–S NRs.

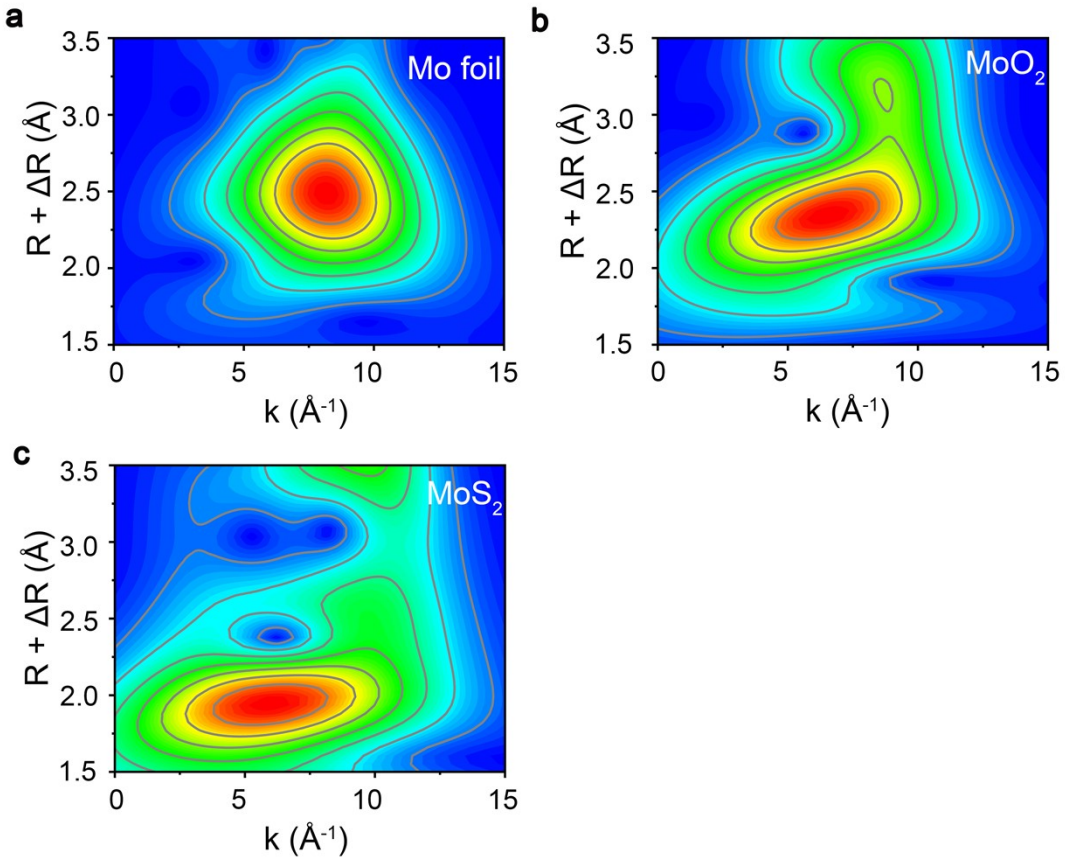

Figure S2. Wavelet Transform Diagram of Sample Mo（Morlet wavelet, η=10, σ=1, k from 2 to 11.10 $Å^{-1}$）

After sulfur doping, two Mo–O bonds, two Mo–Mo bonds and one Mo–S bond existed in the samples. Mo K-edge EXAFS analysis showed that sulfur doping produced Mo–S bonds at *R* = 2.41 nm and Mo–Mo bonds at R = 3.01 nm. The EXAFS results demonstrated that the as–prepared MoO_x–S NRs had structural components similar to those of MoS_2. The introduction of sulfur led to the formation of Mo–S bonds and lattice distortion compared to MoO_2.This alteration in the local coordination structure may be the key factor driving the material's reconstruction from zero-dimensional nanoparticles to more complex nanorings with topological structures. Additionally, in

the k-space, the oscillatory signal characteristics of M–O–S also undergo alteration, further confirms that sulfur doping not only regulates the material's geometric configuration, its electronic structure has also been modified.

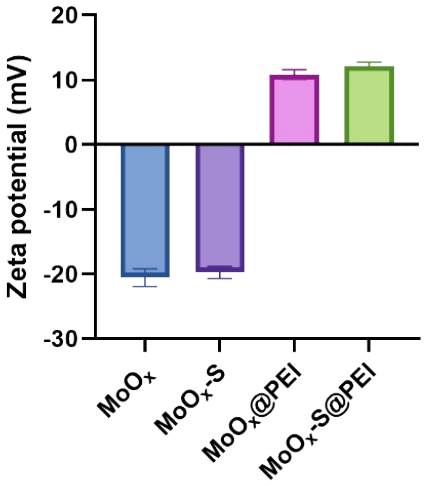

Figure S3. ζ potentials of MoO_x NPs, MoO_x–S NRs, PEI@ MoO_x NPs and PEI@MoO_x–S NRs.

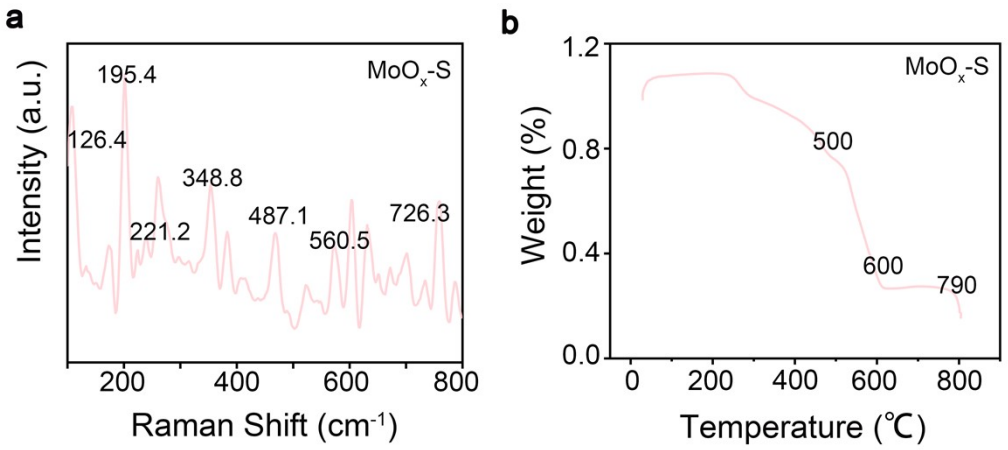

Figure S4. (a) Raman spectrum of MoO_x–S NRs. (b) TGA curve of MoO_x–S NRs.

In the Raman spectrum, the signals at 560.5 and 726.3 cm^{-1} are characteristic of the vibrational mode of molybdenum oxide, and the rest of the peaks including 126.4, 195.4, 221.2, 348.8, and 487.1 cm^{-1} are slightly shifted from the standard values of the MoO_2 sample, which may be attributed to the amorphous structure due to sulfur doping. In the TGA, between 500 ℃ and 600 ℃, there is a sharp decrease in weight due to decomposition of the organic surfactant, and at around 790 ℃, there is another sharp decrease in the weight percentage, which suggests that the molybdenum oxide has sublimated.

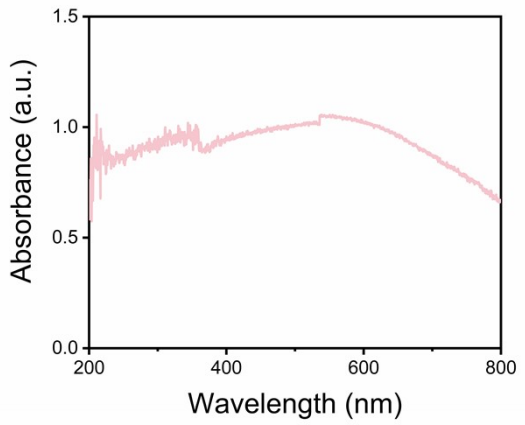

Figure S5. The UV–vis diffuse reflectance spectra of MoO_x–S NRs.

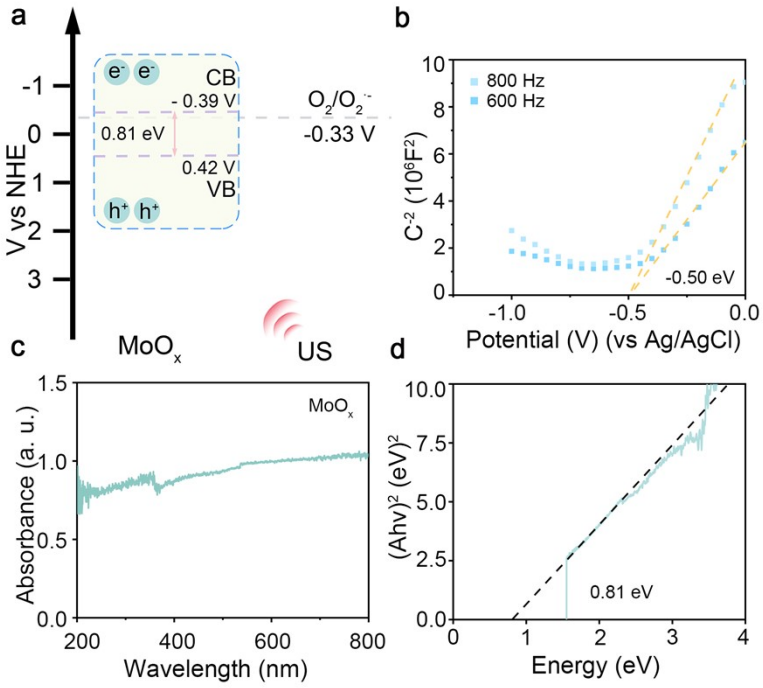

Figure S6. The bandgap and UV–vis diffuse reflectance spectra of MoO_x NPs. (a) Energy band structure of MoO_x NPs. (b) Mott-Schottky plots of MoO_x NPs. (c) The UV–vis diffuse reflectance spectra of MoO_x NPs. (d) The bandgap of MoO_x NPs determined using Kubelka–Munk equation.

The flat–band potential of the MoO_x–S NRs was calculated as –1.12 V (compared to Ag/AgCl, pH = 7), and then, the conduction band potential of the MoO_x–S NRs was converted to –0.51 V (relative to NHE, pH = 7). The flat–band potential of the MoO_x NPs was calculated as –0.50 V (compared to Ag/AgCl, pH = 7), and then, the conduction band potential of the MoO_x–S NRs was converted to –0.39 V (relative to NHE, pH = 7).

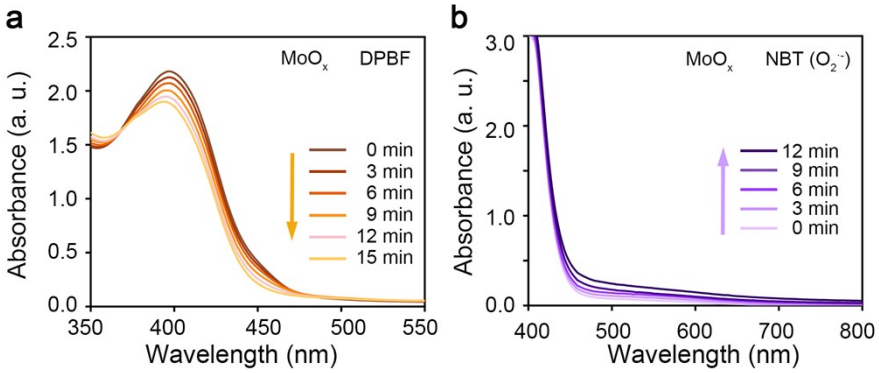

Figure S7. (a) Time–dependent absorbance changes of DPBF in MoO_x NPs with US irradiation. (b) Time–dependent absorbance changes of NBT in MoO_x NPs with US irradiation.

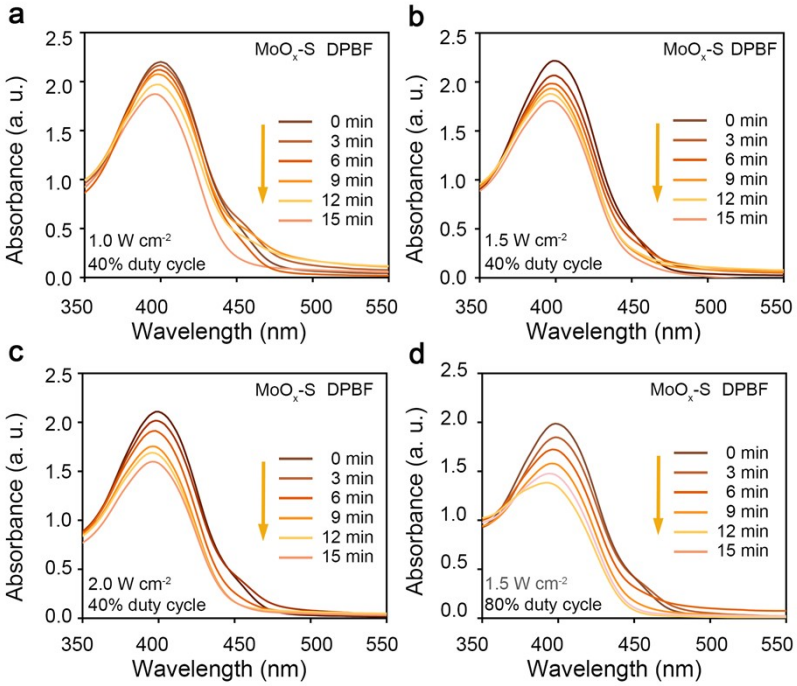

Figure S8. MoO_x–S NRs was detected using DPBF Ultrasonic generation of ROS with different ultrasonic parameters. (a) 1.0 W cm^{-2}, 40% duty cycle; (b) 1.5 W cm^{-2}, 40% duty cycle; (c) 2.0 W cm^{-2}, 40% duty cycle; (d) 1.5 W cm^{-2}, 80% duty cycle.

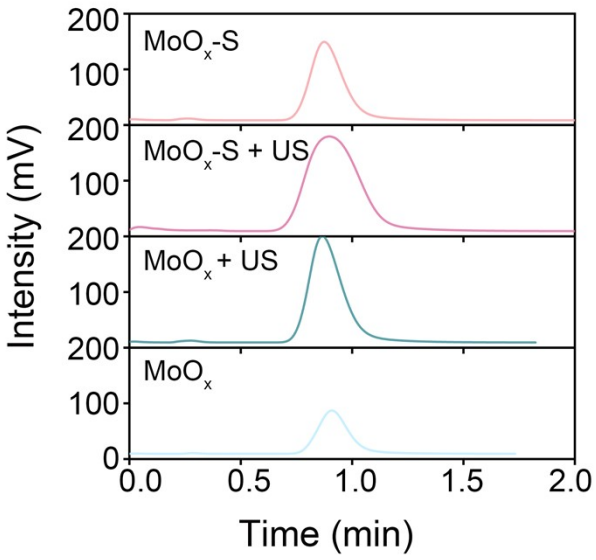

Figure S9. Gas chromatogram of H_2 generated by MoO_x NPs and MoO_x–S NRs in different conditions.

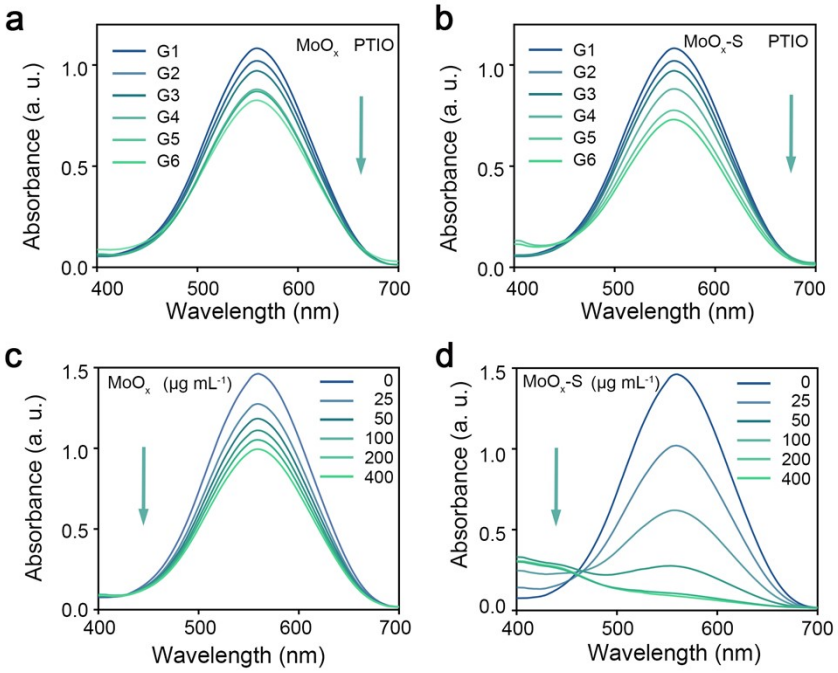

Figure S10. The degradation of PTIO by (a) MoO_x NPs and (b) MoO_x–S NRs under different conditions. G1: Control, G2: H_2O_2, G3: H_2O_2 + US, G4: material, G5: material + H_2O_2, G6: material + H_2O_2 + US (The material concentration was 100 μg mL^{-1}, the ultrasound parameter was 1.5 W cm^{-2}, 40% duty cycle, and the duration was 12 min). The degradation of PTIO (c) MoO_x NPs and (d) MoO_x–S NRs of different concentrations under ultrasonic conditions (The reaction conditions were material + H_2O_2 + US, the ultrasound parameter was 1.5 W cm^{-2}, 40% duty cycle, and the duration was 12 min).

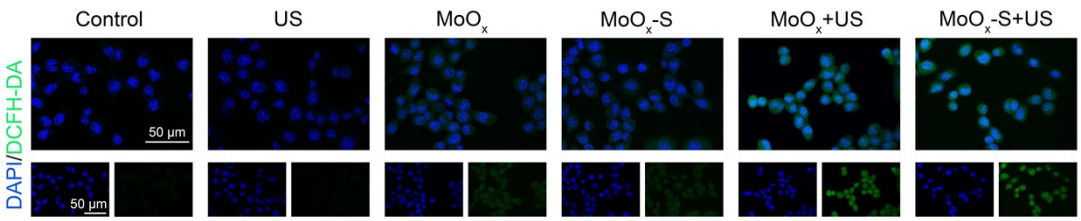

Figure S11. CLSM images of the associated mean fluorescence intensity of intracellular ROS level under various conditions.

Intracellular ROS levels were observed by confocal laser scanning microscopy using a 2,7–dichlorofluorescein diacetate (DCFH–DA) probe. No obvious green fluorescence was detected in the control and US groups, while the MoO_x NPs and MoO_x–S NRs, MoO_x NPs + US and MoO_x–S NRs + US groups showed obvious green fluorescence. Among them, the cells treated with MoO_x–S NRs + US group showed the strongest green fluorescence. The green fluorescence was a result of the oxidation of DCFH to DCF by ROS and was proportional to the concentration of ROS. This confirms that the MoO_x–S NRs + US group has the strongest ability to produce ROS.

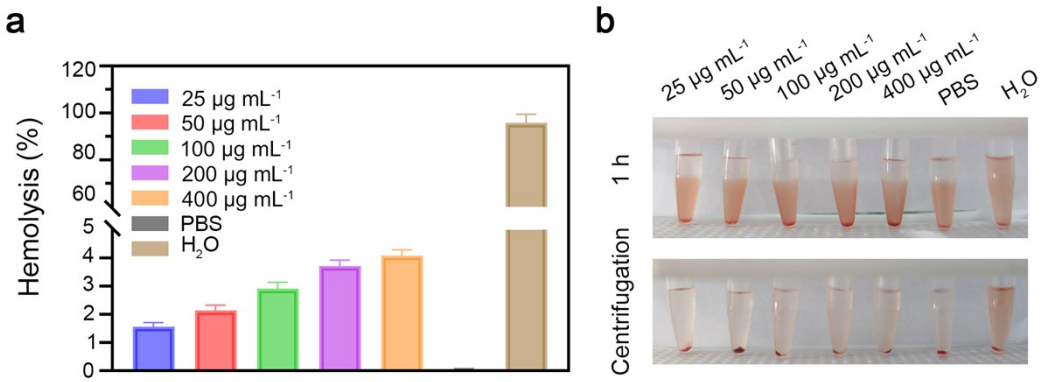

Figure S12. (a) UV–*vis* absorption spectra of supernatant obtained by centrifugation after the co-incubation of blood with MoO_x–S NRs at different concentrations (25, 50, 100, 200 and 400 μg mL^{-1}), H_2O as a positive control and PBS as a negative control. (b) Hemolysis analysis of blood incubated with water (positive control) and different concentrations of MoO_x–S NRs (inset is the digital photograph after centrifugation). From the hemolysis experiment, MoO_x–S NRs showed no significant hemolysis effect even the concentration was 400 μg mL^{-1}.

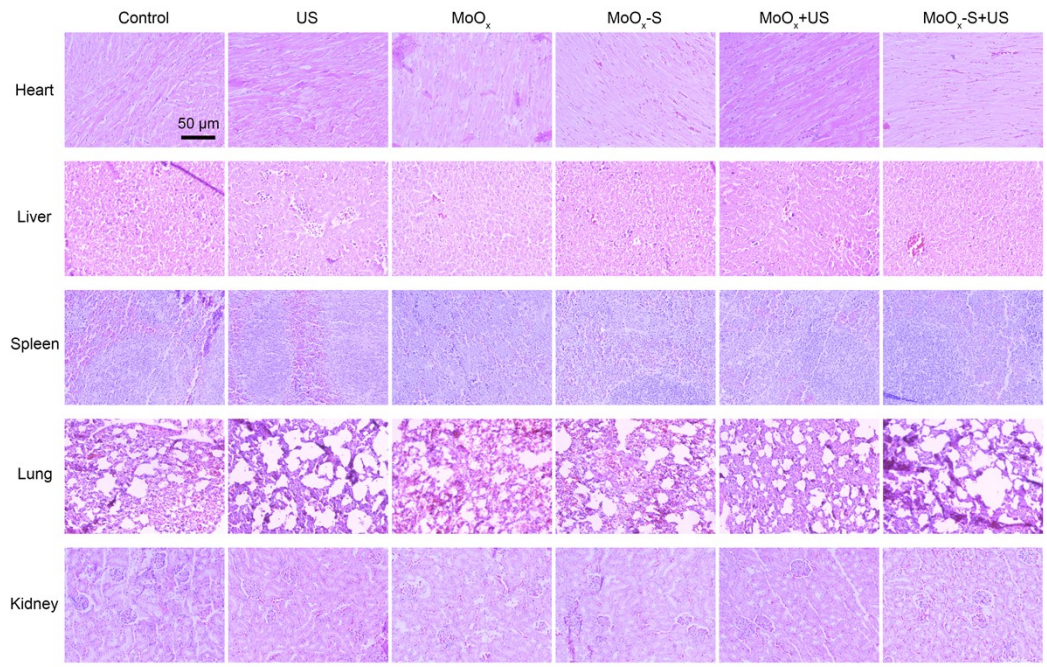

Figure S13. H&E stained tissue sections of major organs (heart, liver, spleen, lung, and kidney) collected from the representative mice in each treatment group. The mice were euthanized after the entire treatment process, and the major organs and tumors were harvested for the H&E staining analysis.

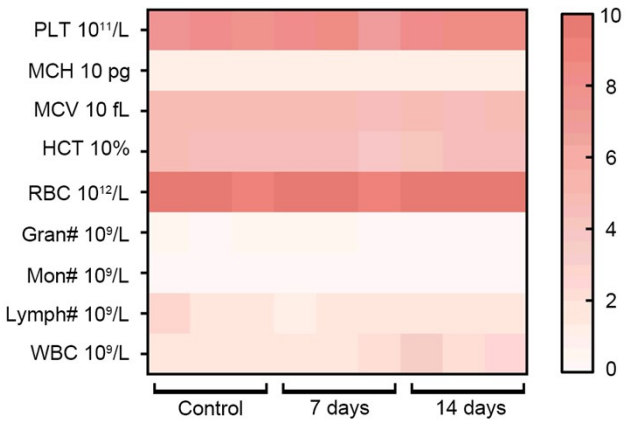

Figure S14. Hematological index of female BALB/c mice with intravenous injection of MoO_x–S NRs after 0, 7, and 14 days.